Beyond the Effect of Particle Size: Influence of CoFe2O4 Nanoparticle Arrangements on Magnetic Properties

ARTICLE *in* CHEMISTRY OF MATERIALS · MAY 2013

Impact Factor: 8.35 · DOI: 10.1021/cm303352r

11 AUTHORS, INCLUDING:

Davide Peddis
Italian National Research Council
64 PUBLICATIONS **820** CITATIONS
SEE PROFILE

Carla Cannas
Università degli studi di Cagliari
100 PUBLICATIONS **1,717** CITATIONS
SEE PROFILE

Anna Musinu
Università degli studi di Cagliari
121 PUBLICATIONS **2,689** CITATIONS
SEE PROFILE

Giorgio Piccaluga
Università degli studi di Cagliari
141 PUBLICATIONS **3,406** CITATIONS
SEE PROFILE

CHEMISTRY OF MATERIALS

Article

pubs.acs.org/cm

Beyond the Effect of Particle Size: Influence of $CoFe_2O_4$ Nanoparticle Arrangements on Magnetic Properties

D. Peddis,*[,†] C. Cannas,[‡] A. Musinu,[‡] A. Ardu,[‡] F. Orrù,[‡] D. Fiorani,[†] S. Laureti,[†] D. Rinaldi,[∇,⊥] G. Muscas,[†,§] G. Concas,[§] and G. Piccaluga[‡]

[†]Consiglio Nazionale delle Ricerche (CNR)−Istituto di Struttura della Materia 00016, Monterotondo Scalo (RM), Roma, Italy

[‡]Dipartimento di Scienze Chimiche e Geologiche, Università di Cagliari Cittadella Universitaria di Monserrato, bivio per Sestu, 09042, Monserrato, Italy and INSTM

[§]Dipartimento di Fisica dell'Università di Cagliari, Cittadella Universitaria di Monserrato, bivio per Sestu, 09042, Monserrato, Italy

[∇]Dipartimento di Fisica e Ingegneria dei Materiali e del Territorio, Università Politecnica delle Marche, via Brecce Bianche 60131, Ancona, Italy

[⊥]Consorzio Nazionale Interuniversitario per le Scienze Fisiche della Materia (CNISM), Roma, Italy

Supporting Information

ABSTRACT: This paper focuses on the magnetic properties of $CoFe_2O_4$ nanoparticles, discussing the influence of nanoparticles arrangements obtained by different synthesis methods. Using high thermal decomposition (HTD) and direct micellar (DM) routes, three samples of $CoFe_2O_4$ nanoparticles with equal primary particle size (∼5 nm) were prepared. The HTD method allows one to obtain highly crystalline primary nanoparticles coated by oleic acid organized in a self-assembling arrangement ($ACoFe_{HTD}$). The DM method results to be appropriate to prepare either irregular arrangements ($IACoFe_{DM}$) or spherical iso-oriented nanoporous assemblies ($SACoFe_{DM}$) of primary $CoFe_2O_4$ nanocrystals. Despite the same particle size, magnetization measurements of the HTD sample show a tendency toward cubic anisotropy ($M_r/M_s \approx 0.7$), while in DM samples, a uniaxial anisotropy ($M_r/M_s \approx 0.4$) is observed. The comparison between $IACoFe_{DM}$ and $SACoFe_{DM}$ samples indicates that the ordering of nanocrystals at the mesoscopic scale induces an increase of the coercive field ($\mu_0 H_c \approx 1.17$ T → $\mu_0 H_c \approx 1.45$ T) and of the reduced remanent magnetization ($M_r/M_s \approx 0.4 \rightarrow M_r/M_s \approx 0.5$). The reason for these differences is discussed. In particular, a detailed study on interparticle interactions is carried out, highlighting the influence of the molecular coating and the formation of spherical iso-oriented assemblies.

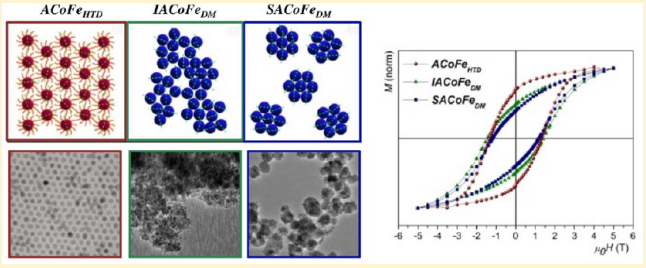

KEYWORDS: *cobalt ferrite, interparticle interactions, orientation easy axis, nanoparticle arrangments*

1. INTRODUCTION

The magnetic properties are very sensitive to the particle size, being determined by finite size effects on the core properties, related to the reduced number of spins cooperatively linked within the particle, and by surface effects, which become more and more important as the particle size decreases.[1,2]

The energy of a magnetic particle is generally dependent on the magnetization direction, and, for uniaxial anisotropy and easy axis aligned with the direction of external field (H), it can be written as[3]

$$E_a = K_a V \sin^2 \theta - M_s V H \cos \theta \quad (1)$$

where K_a is the anisotropy constant, V the particle volume, M_s the saturation magnetization, and θ the angle between magnetization vector and easy direction. According to the Néel−Brown theory,[4,5] above a certain temperature (the blocking temperature, T_B) and on a certain time scale, the particle moment can produce a thermally activated transition. This behavior is analogous to paramagnetism, but with different time and magnetization scale; for this reason, it is called "superparamagnetism". Below T_B, the particle's moment is blocked and unable to rotate over the barrier in the time of a measurement.

The tuning of the magnetic properties of nanoparticles (e.g., T_B, magnetic anisotropy) means control of the energy profile of the "*single*" nanoparticle. Equation 1 shows that E_a is proportional to V and K_a, where the latter is mainly dependent on the structure and chemical composition of the material (i.e., magnetocrystalline and magnetostatic anisotropy).

The magnetic behavior of nanoparticle's assembly is also strongly affected by interparticle interactions that can be dipole−dipole or exchange coupling between surface atoms. The nature and strength of interparticle interactions depend on

Received: October 17, 2012
Revised: March 29, 2013
Published: May 7, 2013

the "arrangement" of nanoparticles. The coating[6,7] with a molecular shell allows to prevent aggregation between nanoparticles and then to reduce interparticle exchange coupling, as well as to control the dipolar interactions by affecting the distances between the particles. This is of paramount importance in 2D and 3D ordered nanoparticle superlattices (SPls), which represent a new generation of tailored materials,[8−10] where "a new physics emerges".[11]

In this frame, in the last 20 years, a great number of synthetic strategies, such as sol−gel,[12−14] micellar,[15,16] sonochemistry, hydrothermal processing, aerosol-vapor methods, surfactant-assisted high-temperature decomposition techniques,[17] and their suitable combinations have been proposed to design new magnetic nanostructured materials.[13,18] Among these, surfactant-assisted solution-phase methods (i.e., micellar method and high thermal decomposition of organic precursor) allow one to obtain nanoparticles with controlled particle size, shape, structure, and composition.[9,17,19−22]

Micellar methods have been used to prepare a wide range of magnetic nanoparticles with different shape and size and with a narrow particle size distribution.[15,16,21] In particular, it has been recently proved that the DM method results are appropriate to prepare either individual or 3D spherical nanoparticle superlattices. In fact, the surfactant is recognized to play a fundamental role, inducing the assembling of the primary nanoparticles in secondary organized assemblies, with an iso-oriented and worm-like porous structure.[21,22] Despite the high number of advantages shown by micellar approaches, because of the low synthesis temperature, a low degree of crystallinity, which is strictly related to the experimental conditions, is often observed.

Since 2002,[23] a further advance in the control of microstructural features and crystallinity of nanoparticles has been given by a synthetic strategy based on the high-temperature decomposition (HTD) of metallorganic precursors (acetylacetonates) in the presence of surfactants (oleylamine, oleic acid) in an organic high-boiling-temperature solvent (octadecene, benzyl ether, phenyl ether). The reason of the formation of nanocrystals with a narrow particle size distribution is related to the possibility to separate the nucleation step from the growth of existing nuclei. Therefore, the size of the nanoparticles is strictly related to the metal precursors, the thermal steps, and the surfactant that, during the decomposition process, is adsorbed and desorbed at the surface of the nuclei, influencing the nucleation and growth phenomena.

Despite a lot of work carried out on each synthesis method, careful comparison between nanomaterials prepared by different synthetic approach is still lacking.

The aim of the present paper is to compare morpho-structural and magnetic properties of nanoparticles prepared via the DM and HTD approaches, exploring their potentiality in modifying the nanoparticles arrangements. The HTD method allows one to obtain highly crystalline nanoparticles coated by oleic acid organized in a self-assembling arrangement ($ACoFe_{HTD}$; see Figure 1a). The DM method results to be appropriate to prepare either randomly aggregated primary $CoFe_2O_4$ nanocrystals ($IACoFe_{DM}$; see Figure 1b) or secondary spherical iso-oriented nanoporous assemblies ($SACoFe_{DM}$; see Figure 1c). The synthesis parameters have been chosen to obtain equal mean primary particle size (∼5 nm). Using this methodology, the paper aims to clarify the influence of the synthetic method and the different nanoparticle arrangements on the structural and magnetic properties. In addition, particular attention will be given to interparticle interactions, superparamagnetic relaxation, and magnetic anisotropy, highlighting the role of molecular coating and of the formation of spherical iso-oriented assemblies.

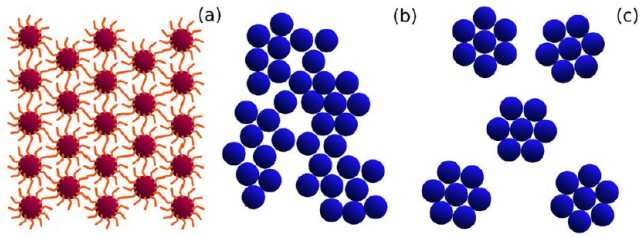

Figure 1. Sketches of the nanoparticle arrangements in the samples under investigation: (a) $CoFe_2O_4$ nanoparticles prepared via the high-temperature decomposition (HTD) method, coated with oleic acid, self-assembled in a two-dimensional (2D) layer ($ACoFe_{HTD}$); (b) $CoFe_2O_4$ nanoparticles prepared via the direct micellar (DM) synthesis method organized in an irregular arrangement ($IACoFe_{DM}$); and (c) $CoFe_2O_4$ nanoparticles prepared via the DM synthesis method organized in structural iso-oriented spherical assemblies ($SACoFe_{DM}$).

2. EXPERIMENTAL SECTION

2.1. Synthesis. The $ACoFe_{HTD}$ sample was synthesized using iron(III) acetylacetonate cobalt(II) acetylacetonate, 1,2-hexadecanediol, oleic acid, oleylamine, and phenyl ether as solvents. All the reagents were mixed into a three-neck round-bottom flask and under reflux, the mixture were heated gradually to 200 °C and kept at this temperature for 30 min; the temperature was then increased rapidly up to 265 °C and the mixture was maintained at this temperature for 30 min. Finally, the black-colored mixture was cooled to room temperature by removing the heat source.[17,24]

$IACoFe_{DM}$ and $SACoFe_{DM}$ samples were prepared starting by aqueous solutions containing $CoCl_2{\cdot}6H_2O$ and $FeCl_2{\cdot}4H_2O$ mixed in a 1:2 molar ratio, with a concentration of iron precursor salt of 0.01 M. To form the mixed normal micelles, the cation mixture was added to an aqueous solution of sodium dodecyl sulfate (SDS) (Aldrich, 98%) and constantly stirred at room temperature for 30 min. Methylamine solution was then added, and the dark slurry was stirred for 3 h at 50 °C. The precipitate, cooled to room temperature, contained spherical iso-oriented aggregates of nanoparticles ($SACoFe_{DM}$). The DM sample was washed with diluted ammonia and submitted to a different number of washing and centrifugation cycles to remove the surfactant. Finally, the powder was dried overnight in an oven at 70−80 °C ($IACoFe_{DM}$).

2.2. Experimental Techniques and Data Treatments. The samples were characterized by XRD, using a Seifert diffractometer with $\theta-\theta$ Bragg−Brentano geometry, using Cu Kα wavelength radiation. The mean dimension, $\langle D_{XRD}\rangle$, of crystalline coherent domains (i.e., crystallite) was obtained using Scherrer's equation:

$$\langle D_{XRD}\rangle = \frac{K\lambda}{\beta \cos\theta} \qquad (2)$$

where K is a constant related to the crystallite shape ($K = 0.9$) and β is the pure breadth of the powder reflection free of the broadening due to instrumental contributions. This calibration was performed by means of the spectrum of a standard Si sample and using the Warren correction.[25]

Cobalt-ferrite nanoparticles were observed in electron micrographs obtained with a TEM system (JEOL, Model 200CX) operating at 200 kV. Finely ground samples were dispersed in octane and submitted to an ultrasonic bath and the suspensions were then dropped on carbon-coated copper grids. The average particle size was obtained using bright-field images measuring the average diameter on over 200 particles in different parts of the grid. The standard deviation (σ) is calculated from the following equation:

$$\sigma = \left\{ \sum \frac{[n_i(D_i - \langle D \rangle)^2]}{N} \right\}^{1/2} \quad (3)$$

where $\langle D_{TEM} \rangle$ is the mean value of the diameter, D_i the diameter of particle i, and N the number of the particles. HRTEM images were obtained with a JEM 2010 UHR equipped with a Gatan imaging filter (GIF) and a Gatan Model 794 slow scan CCD camera.

The DC magnetization measurements were performed by a Quantum Design SQUID magnetometer, equipped with a superconducting coil that produces magnetic fields in the range from ± 5 T. Samples in the form of powders were immobilized in an epoxy resin to prevent any movement of the nanoparticles during the measurements. Magnetization versus temperature measurements were performed using zero-field-cooled (ZFC), field-cooled (FC), and thermoremanent magnetization (TRM) protocols. ZFC and FC magnetization measurements were carried out by cooling the sample from room temperature to 5 K in zero magnetic field; then, a static magnetic field of 2.5 mT was applied. M_{ZFC} was measured during the warmup from 5 K to 300 K, whereas M_{FC} was recorded during the subsequent cooling. In the TRM measurements, the sample was cooled from 300 K to 5 K in an external magnetic field of 2.5 mT; then, the field was turned off and the magnetization was measured upon warmup. The field dependence of remanent magnetization was measured using the isothermal remanent magnetization (IRM) and direct current demagnetization (DCD) protocols. The initial state for an IRM measurement is a totally demagnetized sample cooled in zero magnetic field. In the present case, an external field was applied for 10 s; then, it was switched off and the remanence was measured (M_{IRM}). The process was repeated, increasing the field up to saturation. In a DCD measurement, the initial state is the magnetically saturated one. An external field of −5 T was applied for 10 s; then, a small external field in the direction opposite to magnetization was applied and, after 10 s, it was switched off and the remanent magnetization (M_{DCD}) was measured. This was repeated while increasing the field up to +5T. Because of the fairly subtle differences in some magnetic features, it should be emphasized that the reproducibility of all of the measurements was carefully verified.

AC magnetic measurements have been performed by a Quantum Design PPMS AC/DC magnetometer. The mutual inductance system allows high accuracy. Data have been taken on warming, after zero field cooling, varying the frequency (f), in the range of 10 Hz to 10 kHz without static superimposed magnetic field. The real (χ') and the imaginary (χ'') values of the complex susceptibility have been evaluated, taking into account the demagnetizing effects.

3. RESULTS

TEM analysis for the $ACoFe_{HTD}$ sample shows primary nanoparticles with diameters of ∼5 nm self-assembled in a hexagonal close-packed (hcp) superlattice (see Figure 2a). The presence of the oleic acid−oleylamine coating at the nanoparticle surface keeps them isolated from each other, via a layer ∼2 nm thick. High-resolution TEM images (Figure 2b) show an almost-spherical particle ∼5 nm in diameter, oriented along the [220] plane of the cobalt ferrite structure, confirming the high degree of cristallinity of the material.[24]

TEM analysis of the $SACoFe_{DM}$ sample indicates the presence of 5-nm nanoparticles arranged in spherical aggregates with an average size of ∼40−60 nm exhibiting a worm-like nanoporous structure (Figure 2e); the images obtained in high-resolution mode (Figure 2f) show an iso-oriented structure comprised of primary building blocks of almost-spherical particles.[9,21] An irregular arrangement, typical of nanopowders, is observed for the surfactant-free sample ($IACoFe_{DM}$) (Figure 2c,d).[21] TEM analysis indicates that the average particle diameter and standard deviation σ, calculated by eq 3 (see Table 1) are equal, within experimental error, in samples

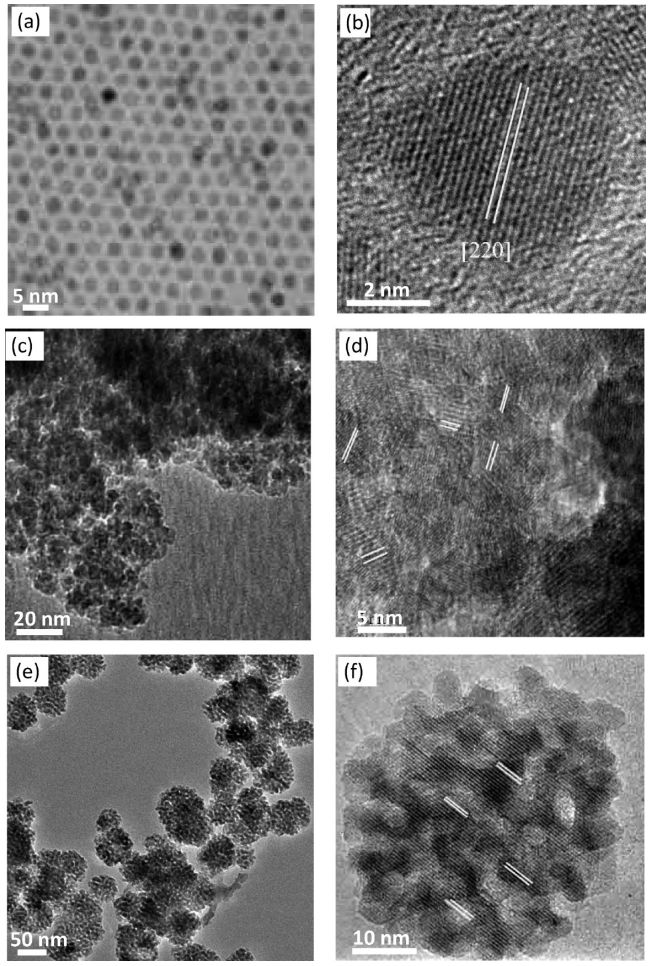

Figure 2. TEM and HRTEM images of $ACoFe_{HTD}$ sample (panels a and b, respectively), $IACoFe_{DM}$ (panels c and d, respectively), and $SACoFe_{DM}$ (panels e and f, respectively) samples.

Table 1. Mean Particle Size from TEM Data ($\langle D_{TEM} \rangle$), Polydispersity (σ), Mean Particle Size form XRD Pattern ($\langle D_{XRD} \rangle$), Temperature Corresponding to the Maximum in ZFC Curve (T_{max}); Irreversibility Temperature (T_{irr}), Blocking Temperature from TRM Measurement (T_B)

sample	$\langle D_{TEM} \rangle$ (nm)	σ (%)	$\langle D_{XRD} \rangle$ (nm)	T_{max} (K)	T_{irr} (K)	T_B (K)
$ACoFe_{HTD}$	4.6(1)	26	5.0(2)	207(5)	247(5)	120(3)
$IACoFe_{DM}$	4.8(3)	23	3.9(4)	224(4)	285(4)	154(4)
$SACoFe_{DM}$	4.8(3)	23	4.5(4)	220(3)	283(5)	157(3)

prepared via the DM ($IACoFe_{DM}$, $SACoFe_{DM}$) and HTD synthetic approaches, as confirmed by the particle size distribution reported in Figure S1b in the Supporting Information. It should be emphasized that, since $IACoFe_{DM}$ and $SACoFe_{DM}$ are obtained from the same sample batch, the particle size distributions are the same for the two samples.

The X-ray diffraction (XRD) patterns in Figure S1b in the Supporting Information confirm TEM investigation, showing Bragg reflections corresponding to those of a single $CoFe_2O_4$ phase with a cubic spinel structure (JCPDS File Card No. 246 22-1086). No peak of any other phase was detected. Using the Debye−Scherrer formula (eq 2) on the [400] reflection, the average coherent domains was obtained (see Table 1).

dx.doi.org/10.1021/cm303352r | Chem. Mater. 2013, 25, 2005−2013

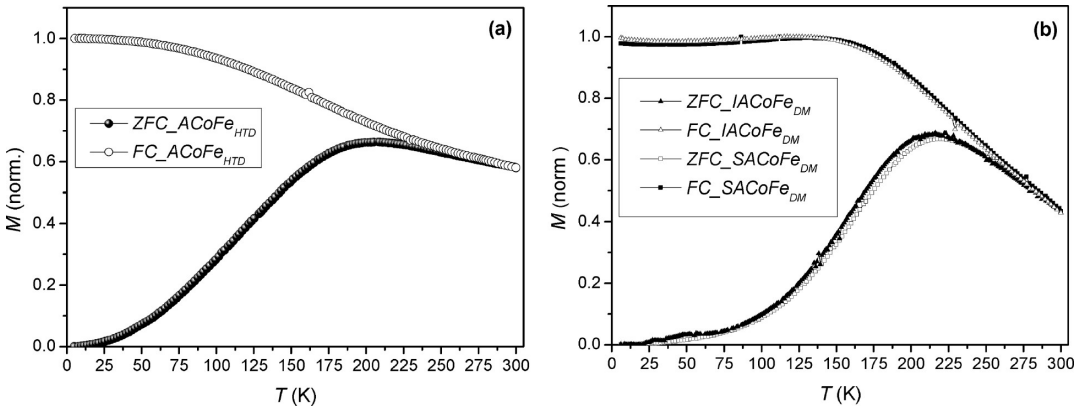

Figure 3. ZFC (solid symbols) and FC (empty symbols) magnetizations for (a) $ACoFe_{HTD}$ (circles) and (b) $IACoFe_{DM}$ (triangles) and $SACoFe_{DM}$ (squares) samples.

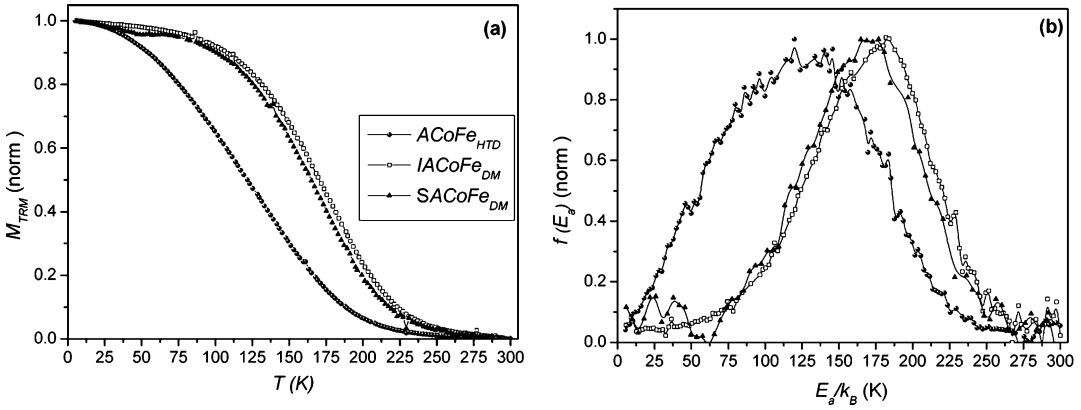

Figure 4. (a) TRM magnetizations and (b) corresponding distribution of magnetic anisotropy energy for (●) $ACoFe_{HTD}$, (□) $IACoFe_{DM}$, and (▲) $SACoFe_{DM}$.

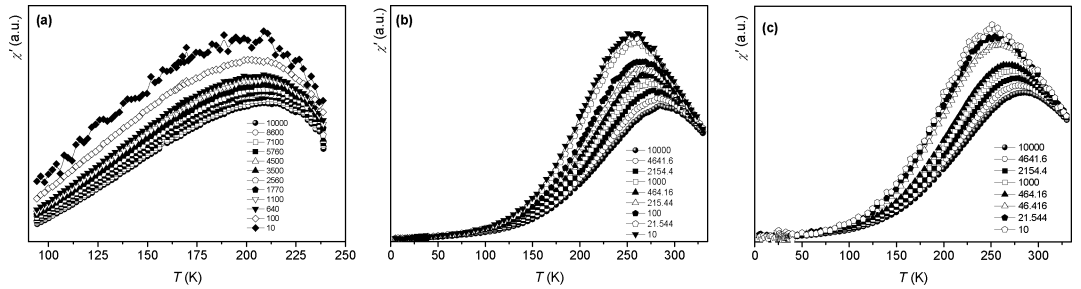

Figure 5. Temperature dependence of the in-phase component of the ac susceptibility (χ') at different frequencies for (a) $ACoFe_{HTD}$, (b) $IACoFe_{DM}$, and (c) $SACoFe_{DM}$ samples.

Magnetic properties were investigated by the temperature and field dependence of magnetization. ZFC and FC magnetization measurements on HTD and DM samples are reported in Figures 3a and 3b, respectively. ZFC curves exhibit a maximum at a temperature (T_{max}) that, for noninteracting particles, is directly proportional to the average blocking temperature, with a proportionality constant of $\beta = 1 - 2$, depending on the type of particle size distribution.[26] An irreversible magnetic behavior is observed below a given temperature (T_{irr}) that is related to the blocking of the biggest particles.[27,28] The $IACoFe_{DM}$ and $SACoFe_{DM}$ samples show very similar values of T_{irr} and T_{max}, which are higher than those of the $ACoFe_{HTD}$ sample (see Table 1). In all of the samples, the FC magnetization increases as the temperature decreases, down to a temperature below which M_{FC} exhibits a temperature-independent behavior, revealing the presence of interparticle interactions, leading to a frozen magnetic ordered state with high anisotropy.[5] In the DM samples, a plateau of FC magnetization is observed just below T_{max}, similar to that observed in a spin-glass system. TRM magnetization curves (see Figure 4a) show a decrease with increasing temperature, as expected for an assembly of magnetic monodomain particles. For noninteracting particles, the term dM_{TRM}/dT gives an estimate of the anisotropy energy barrier distribution:[29]

$$f(E_a) \propto -\frac{dM_{TRM}}{dT} \tag{4}$$

Because of the presence of interparticle interactions in our samples, the derivative of M_{TRM} (Figure 4b) can actually be considered only as a rough estimation of the E_a distribution.

dx.doi.org/10.1021/cm303352r | Chem. Mater. 2013, 25, 2005−2013

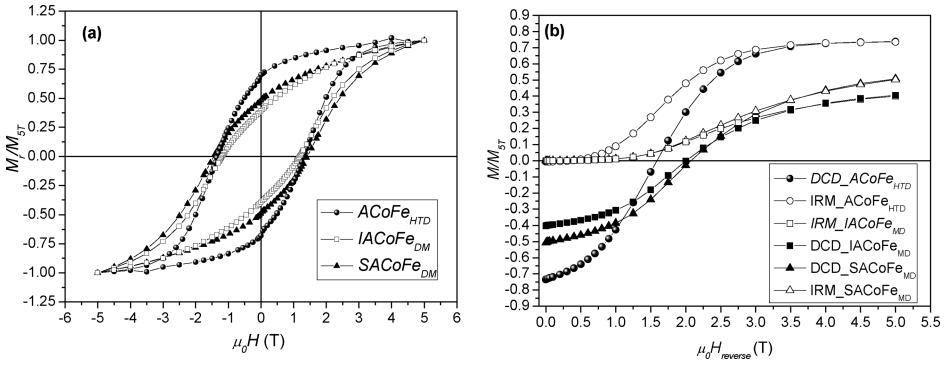

Figure 6. (a) Hysteresis loops recorded at 5 K for (●) $ACoFe_{HTD}$, (□) $IACoFe_{DM}$, and (▲) $SACoFe_{DM}$ samples. (b) DCD (full symbols) and IRM (empty symbols) remanence magnetization for $ACoFe_{HTD}$ (circles), $IACoFe_{DM}$ (squares), and $SACoFe_{DM}$ (triangles) samples.

Table 2. Mean Particle Size from TEM Data ($\langle D_{TEM}\rangle$), Saturation Magnetization (M_s), Reduced Remanent Magnetization (M_r/M_s), Coercive Field ($\mu_0 H_c$), Theoretical Coercive Field Calculated by Equation 9 ($\mu_0 H_{c\_Th}$), Interaction Field ($\mu_0 H_{int}$), Interaction Dipolar Energy (E_{dip}/k_B)

sample	$\langle D_{TEM}\rangle$ (nm)	M_s (A m^2 kg^{-1})	M_r/M_s	$\mu_0 H_c$ (T)	$\mu_0 H_{c\_Th}$ (T)	$\mu_0 H_{int}$ (T)	E_{dip}/k_B (K)
$ACoFe_{HTD}$	4.6(1)	70(2)	0.68	1.29(3)	$1.34_{CA}(3)$	0.0650	8.0(5)
$IACoFe_{DM}$	4.8(3)	54(3)	0.39	1.17(3)	$1.08_{UA}(2)$	0.195	34(4)
$SACoFe_{DM}$	4.8(3)	51(3)	0.48	1.45(4)		0.189	32(4)

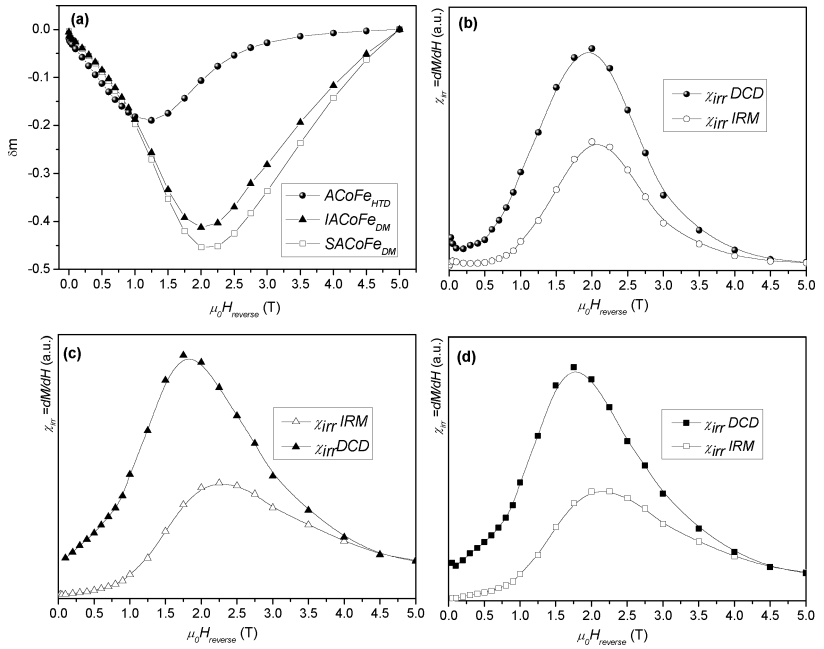

Figure 7. (a) δM plots for (●) $ACoFe_{HTD}$, (□) $IACoFe_{DM}$, and (▲) $ACoFe_{DM}$ samples. Also shown are plots of the irreversible susceptibility ($\chi_{irr} = dM/dH$) derived by (●) DCD and (○) IRM for the (b) $ACoFe_{HTD}$, (c) $IACoFe_{DM}$, and (d) $SACoFe_{DM}$ samples.

Within the Néel model, the blocking temperature can be defined as the temperature for which the relaxation time is equal to the measuring time of the experimental technique. In a real system of nanoparticles, where a finite size distribution always exist, T_B is often defined as the temperature at which 50% of the sample is in the superparamagnetic state.[7] Since T_B is proportional to E_a, an estimate of the T_B distribution can be obtained from the E_a distribution by evaluating the temperature at which 50% of the particles overcome their anisotropy energy barriers (Table 1). The T_B values follow the same trend of T_{max} and T_{irr}.

The AC susceptibility measurements represent a powerful tool to investigate magnetic transitions. The temperature dependence of the in-phase component (χ') recorded with ZFC protocol (Figure 5) confirms the results of the DC magnetization measurements, showing a peak with a corresponding temperature (T_{m_ac}) that increases as the frequency increases for all of the samples.

The field dependence of magnetization was studied at low temperature (Figure 6), and the saturation magnetization (M_s), reduced remanent magnetization (M_r/M_s), and coercive field (H_c) extracted from hysteresis loops are reported in Table 2. $ACoFe_{HTD}$ shows a M_s value close to the bulk one (83−90 A m^2 kg^{-1}), while a strong decrease of saturation magnetization in both DM samples is observed. This can be ascribed to a low

dx.doi.org/10.1021/cm303352r | Chem. Mater. 2013, 25, 2005−2013

degree of crystallinity associated to the low synthesis temperature (50 °C) used in the DM method.

A more-complex trend is shown by reduced remanent magnetization and coercivity. A M_r/M_s value close to that expected for nanoparticle with cubic anisotropy (~0.8) is shown by $ACoFe_{HTD}$, while a decrease is observed in samples prepared by micellar route. In addition, an increase in M_r/M_s is observed in the $SACoFe_{DM}$ (~0.5) sample, with respect to that of $ACoFe_{DM}$ (~0.4). The formation of spherical aggregates (i.e., $SACoFe_{DM}$) induces an increase of anisotropy, leading to a value of H_c that is higher than that of both $ACoFe_{HTD}$ and $IACoFe_{DM}$ samples. In order to gain deeper insight into a quasi-static magnetic properties of the materials, the dependence of remanent magnetization, recorded with DCD and IRM protocols, was investigated at low temperature (5 K). The trend $M_{DCD(5T)}/M_s$ and $M_{IRM(5T)}/M_s$, reported in Figure 6b, confirms the trend of M_r/M_s extracted by hysteresis loops.

4. DISCUSSION

Structural and morphological characterization indicates that DM and HTD synthesis approaches are effective in the preparation of uniform $CoFe_2O_4$ nanoparticles with mean primary particle size of ~5 nm, equal within experimental error. The DM method results to be also appropriate for the achievement of iso-oriented spherical aggregates of primary nanoparticles. The surfactant is recognized to play a fundamental role, since, in the presence of SDS, the formation of spherical aggregates is observed and when the surfactant is completely removed, both iso-orientation of the primary nanoparticles and the regular spherical shape are lost.[21]

4.1. Interparticle Interactions. In this complex framework, it can be inferred that the major role in the collective physical behavior of magnetic nanoparticles organized in different arrangements is played by the type and the strength of interparticle interactions. The analysis of remanent magnetization curves measured by IRM and DCD protocols allows us to investigate the interaction regime among particles (see the Supporting Information for a detailed description). The two field-dependent remanent magnetizations are related by the Wohlfarth equation:

$$\delta m = m_{DCD} - (1 - 2m_{IRM}) \quad (5)$$

where $m_{DCD}(H)$ and $m_{IRM}(H)$ are both normalized to the remanent magnetization after saturation.

In particular, a negative deviation from the linearity condition is evidence of the predominance of dipole−dipole interactions, while a positive deviation can be attributed to the predominance of exchange interactions. The δm plots (Figure 7a) indicate, for all the samples, the prevalence of dipolar interactions; it is interesting to observe that, despite the absence of molecular coating, DM samples do not show any experimental evidence of exchange coupling between atoms located at the nanoparticle surface. This result is in agreement with a recent deep study on the same type of samples, which excludes the presence of exchange interactions.[10] The application of this procedure to particles with cubic anisotropy (i.e., $ACoFe_{HTD}$ sample) is not trivial, because δm plots, calculated for randomly oriented noninteracting particles with cubic anisotropy, deviate from linearity toward "positive" values.[30,31] On the other hand, the remanence curve technique (defined for systems of uniaxial anisotropy) has been often applied, without any modification, to systems consisting of particles with mixed multiaxial and uniaxial anisotropy.[32]

The analysis of magnetic interactions among particles can be further improved calculating, as a first approximation, a mean value of interactions field between the particles.[10,33]

$$H_{int} = \frac{(H_r' - H_r)}{2} \quad (6)$$

H_r' and H_r correspond to the position of the maxima of the field derivative of $m_{DCD}(H)$ and $m_{IRM}(H)$ curves (i.e., maxima in the irreversible susceptibility, which maps the switching field distribution) reported in Figures 7b, 7c, and 7d for $ACoFe_{HTD}$, $IACoFe_{DM}$, and $SACoFe_{DM}$, respectively. Interaction field values (see Table 2) confirm the presence of demagnetizing interactions in all of the samples. The H_{int} values are equal, within experimental error, in both DM samples and they are smaller for the $ACoFe_{HTD}$ sample, indicating weaker interparticle interactions in this sample. Considering the prevalence of dipolar interactions, the difference in the strength of interactions between the HTD and DM samples can be discussed, taking into account the balance between the increase of interparticle distance (i.e., the presence of molecular coating in $ACoFe_{HTD}$) and the variation of saturation magnetization. In fact, in a sample of randomly distributed nanoparticles, assuming a point dipole model (i.e., center to center maximum distance), a mean value of dipolar energy E_d/k_B (Table 2) can be calculated.[34] Both DM samples show a dipolar energy higher than that $ACoFe_{HTD}$ sample.

4.2. Supermagnetism. The "*supermagnetic*" behavior[35] of the samples must be discussed in the framework defined by interparticle interactions. DM samples show T_{max}, T_{irr}, and T_B values higher than those of the HTD sample, despite having the same primary particle size. This can be ascribed to the increase of interparticle interactions, leading to higher values of blocking temperature in samples prepared by the micellar route. $SACoFe_{DM}$ and $IACoFe_{DM}$ show substantially equal values of T_{max}, T_{irr}, and T_B, indicating that the arrangement of nanoparticles in spherical aggregates does not induce relevant modification in the supermagnetic behavior. Nevertheless, as already observed by Pileni and co-workers, the ZFC peak is slightly narrower for the ordered sample,[11] indicating a narrower distribution of blocking temperatures in $SACoFe_{DM}$. Since the $IACoFe_{DM}$ and $SACoFe_{DM}$ samples are obtained by the same batch, they have the same particle size distribution (see empty circles in Figure S1a, given in the Supporting Information). Thus, the difference in width of the ZFC peak cannot be ascribed to changes in the size distribution of nanoparticles or in the magnetic anisotropy of the material, but it can be explained by changes in the arrangement of the nanoparticles.[11] An analysis of the remanent magnetization shows a prevalence of dipolar interactions in both DM samples. Dipolar magnetic forces have a strong directional dependence, and, consequently, dipolar interactions in an assembly of nanoparticles are expected to be sensitive to the detailed geometrical arrangement.[11] In the $SACoFe_{DM}$ sample, the geometric environment of the nanoparticles is fairly uniform, while the $IACoFe_{DM}$ sample shows an irregular stacking periodicity. Then, it is reasonable to expect a sharper distribution of dipolar energy and blocking temperatures in the samples of nanoparticles organized in spherical aggregates. We acknowledge that this effect of order is fairly subtle; however, it should be emphasized that it is highly reproducible and it also has already been observed.[11] Further confirmation of this picture is given by the direct comparison of the distribution of switching field obtained by DCD measurements (see Figure

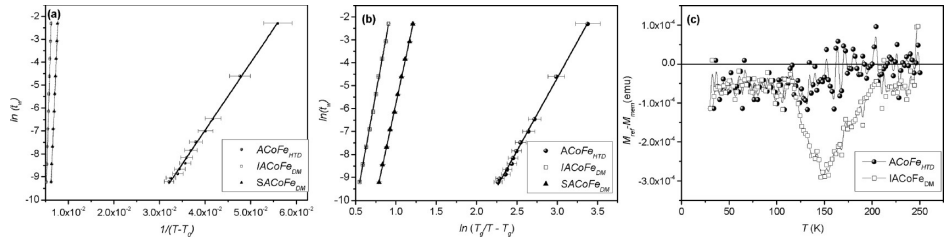

Figure 8. Frequency dependence of T_{max} for (●) ACoFe$_{HTD}$, (□) IACoFe$_{DM}$, and (▲) SACoFe$_{DM}$ in (a) the Vogel–Fulcher model and (b) the power law model. (c) Difference between the ZFC-reference curve and the ZFC-memory curve, with waiting times of 3600 s at 150 K.

Table 3. Left Part: Characteristic Relaxation Time (τ_0), Averaged Energy Barrier (E_a/k_B), and Interparticle Interaction Energy (T_0), Obtained by Vogel-Fulcher Model; Right Part: Characteristic Relaxation Time (τ_0), Exponent that Governs the Critical Divergence of the Relaxation Time (α) at the Glassy Temperature (T_g) Obtained by Power Law Model

	Vogel–Fulcher Model			Power Law Model		
sample	τ_0 (s)	E_a/k_B (K)	T_0 (K)	τ_0 (s)	α	T_g (K)
ACoFe$_{HTD}$	2.94×10^{-10}	287(4)	189(5)	4.98×10^{-11}	6.3(6)	191(5)
IACoFe$_{DM}$	1.26×10^{-12}	2191(180)	169(8)	3.01×10^{-10}	11(2)	221(8)
SACoFe$_{DM}$	1.26×10^{-11}	1616(140)	182(7)	2.16×10^{-10}	11(1)	221(7)

S2a in the Supporting Information) and AC susceptibility measured at different frequency (see Figure S2b in the Supporting Information).

For all of the samples the frequency dependence of T_{m_ac} does not follow the Arrhenius law, which would lead to nonphysical values of characteristic relaxation time ($\tau_0 = 10^{-18}$ s). On the other hand, both the phenomenological Vogel–Fulcher law (eq 7),[36,37] and the power law (eq 8) describe the frequency dependence of T_{max} well for all of the samples.

$$\tau = \tau_0 \exp\left(\frac{E_a/k_B}{T - T_0}\right) \tag{7}$$

$$\tau = \tau_0\left(\frac{T_g}{T - T_g}\right)^{\alpha} \tag{8}$$

The Vogel–Fulcher law describes the temperature dependence of the relaxation time in weakly interacting nanoparticles assemblies, where T_0 represents a qualitative estimate of the interparticle interaction energy. On the other hand, the power law describes the relaxation time in spin-glass systems and strongly interacting assemblies of nanoparticles, showing spin-glass-like features. In eq 8, T_g is the glassy temperature and α is an exponent that governs the critical divergence of the relaxation time at T_g. Figures 8a and 8b show the frequency dependence of T_{m_ac} for ACoFe$_{HTD}$ (full circles), IACoFe$_{DM}$ (empty squares), and SACoFe$_{DM}$ (full triangles) in the Vogel–Fulcher model and the power law model, respectively. Results of the fit are reported in Table 3. From a mathematical point of view, both models describe the frequency dependence of T_{m_ac} well. In order to discriminate between the Vogel–Fulcher model and the power-law model, the possible presence of non-equilibrium dynamics (e.g., memory effect in ZFC magnetization) was investigated. A ZFC reference curve was recorded with the procedure described previously. The memory curves were measured in the same way, but after the sample was maintained in zero field for 3 h at 150 K for DM samples and at 100 K for the HTD sample. A decrease in magnetization is observed only in samples prepared using the DM approach, suggesting a spin-glass-like behavior, in agreement with FC magnetization, showing a plateau below T_{max}. On the other hand, no memory effect is observed in ACoFe$_{HTD}$. As an example, Figure 8c shows the difference curves (ZFC$_{ref}$ − ZFC$_{mem}$) for ACoFe$_{HTD}$ (full circles) and IACoFe$_{DM}$ (empty squares) samples. The data then suggest that the frequency dependence of T_{m_ac} in samples prepared via the DM approach can be better described by the power law model, while the interaction regime present in the ACoFe$_{HTD}$ sample is ascribable to a Vogel–Fulcher scenario.[37] IACoFe$_{DM}$ and SACoFe$_{DM}$ samples exhibit T_g and α values that are equal, within experimental error, in agreement with no-relevant differences observed in interparticle interactions. The critical exponent ($\alpha = 10.7$) is higher than the values usually reported for canonical spin glasses ($\alpha = 7–8$),[36,38] but it is fairly comparable to those reported by interacting nanoparticles exhibiting spin-glass-like behavior.[39]

The dynamical behavior of an assembly of weakly interacting particles was well-described in the literature by the models proposed by Dormann, Fiorani, and Tronc[40] and Hansen and Morup.[28] In our system of particles with weak /medium interaction strengths, the application of these models cannot be straightforward, because the particles are highly anisotropic. This would imply accounting for an important anisotropy energy term.

4.3. Magnetic Anisotropy. Bulk $CoFe_2O_4$ is characterized by a strong cubic anisotropy of magnetocrystalline origin, mainly due to the Co^{2+} ions, which have nonzero orbital momentum.[41] Entering the nanoscale, a coexistence of cubic and uniaxial anisotropy is observed, with a completely uniaxial anisotropy for particle sizes of <5 nm.[24] Generally speaking, the magnetization processes for particles with cubic anisotropy differ from those of a system of particles with uniaxial anisotropy. In fact, because of the presence of six easy directions, the probability that randomly aligned particles have an easy direction close to the direction of the applied field is very high. Therefore, under these conditions, it is expected that a multiaxial system will have increased remanence ($M_r/M_s = 0.8$).[42,32,43,44] From this point of view, interesting differences among the samples are observed in the quasi-static magnetic behavior at low temperature (5 K). The reduced remanent magnetization is ∼0.4 in the IACoFe$_{DM}$ sample, which is consistent with uniaxial anisotropy. On the other hand, the

dx.doi.org/10.1021/cm303352r | Chem. Mater. 2013, 25, 2005–2013

$ACoFe_{HTD}$ sample shows a remanence of $M_r/M_s \cong 0.7$, which suggests a tendency toward cubic anisotropy. This picture can be further confirmed by some calculations. Following the suggestions of Kodama and co-workers, the irreversibility field (H_k) observed in the hysteresis loop can be considered as a good estimation of the anisotropy field H_k.[45] Taking H_k as the field where the difference between magnetizing and demagnetizing branches, normalized to M_s value, becomes <3%, a value of the effective anisotropy constant can be calculated.[42] For a system of noninteracting randomly oriented spherical particles, the coercive field is given by

$$H_{c\_th} = \gamma \frac{K_a}{M_s} \tag{9}$$

where γ is a constant (γ = 0.64 for nanoparticles with cubic anisotropy and γ = 0.5 for nanoparticles with uniaxial anisotropy). Using eq 9, fairly good agreement with experimental values of H_c is obtained for $ACoFe_{HTD}$ and $IACoFe_{DM}$ samples, assuming cubic and unixial anisotropy, respectively (see Table 2). This can be related to different synthesis temperatures used in the HTD (300 °C) and DM (50 °C) approaches, which are responsible for the different degrees of crystallinity. The higher temperature used in HTD synthesis leads to highly crystalline particles (see Figure 2b), justifying the observed tendency toward cubic anisotropy.

The behavior of the $SACoFe_{DM}$ sample should be discussed from a different point of view. Both the reduced remanent magnetization and coercive field for this sample are higher than those of the $IACoFe_{DM}$ sample, and H_c cannot be fairly reproduced by eq 9. This leads one to believe that the different magnetic properties observed in the $SACoFe_{DM}$ sample are related to the organization in spherical aggregates.

Generally speaking, the increase in the reduced remanence magnetization could be attributed either to a partial orientation of the easy axes or to the formation of ferromagnetic domains induced by dipolar interactions. In order to verify the first hypothesis, calculations on the FC magnetization values at low temperature have been performed. In particular, as detailed described in the Supporting Information, the ratio between the FC magnetization of a partially aligned system (M_{FC}^{align}) and the FC magnetization of randomly oriented system (M_{FC}) can be written as

$$M_{FC}/M_{FC}^{align} = 1 + \alpha(3\cos^2\beta - 1) \tag{10}$$

where β is the average angle between the easy magnetic axis and the applied magnetic field and α is the fraction of nanoparticles having aligned easy axes. If all the particles are randomly oriented, α = 0 and M_{FC}/M_{FC}^{align} = 1, while the presence of a fraction of particles with oriented easy axes leads to $M_{FC}/M_{FC}^{align} \neq 1$. The FC magnetization value recorded at 10 K under an applied field of 2.5 mT is different for the $IACoFe_{DM}$ and $SACoFe_{DM}$ samples, giving $M_{FC}^{IACoFe_{DM}}/M_{FC}^{SACoFe_{DM}}$ = 2.06.

This suggests a partial orientation of the easy axes in the $SACoFe_{DM}$ sample. In fact, it is reasonable that the iso-oriented structure present in each aggregate leads to an alteration of the random situation present in the $IACoFe_{DM}$ sample (see Figure 9). The anisotropy of the $CoFe_2O_4$ primary nanoparticles is the same for the $IACoFe_{DM}$ and $SACoFe_{DM}$ systems, since they are obtained by the same synthesis method. The increase of M_r/M_s and H_c then can be ascribed to the partial orientation of the anisotropy easy axis. Assuming that all the easy axes are aligned,

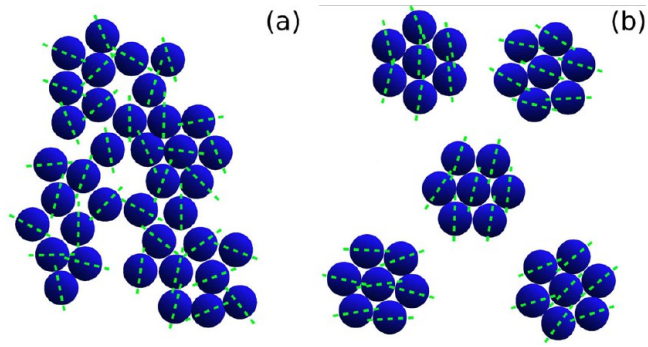

Figure 9. Sketch of the anisotropy easy axis orientation in (a) $IACoFe_{DM}$ and (b) $SACoFe_{DM}$ samples.

the hysteresis loop measured when the field is parallel to the easy axes is expected to be rectangular (M_r/M_s = 1), whereas, along a perpendicular direction (hard direction), it is a straight line with no coercive field (M_r/M_s = 0). Then, for an assembly of nanoparticles with a random distribution of easy axes, the value of M_r/M_s should be ~0.5.[46] Within this model, the increases in reduced remanence magnetization and coercive field observed from the $IACoFe_{DM}$ sample to the $SACoFe_{DM}$ sample can be explained by a partial orientation of easy axes in the iso-oriented spherical aggregates, with respect to the random distribution observed in irregular arrangements of nanoparticles.

CONCLUSIONS

Despite the fact that the magnetic properties of nanoparticles are mostly affected by particle size, other factors, such as magnetic anisotropy and interparticle interactions, can play a fundamental role in the physics of these systems. Magnetic anisotropy depends on, besides the particle size, the structure and chemical composition of the material and then it is strictly related to the synthesis conditions. The nature and the strength of interparticle interactions depend on the geometrical arrangement of nanoparticles and their interparticle distance (e.g., because of the presence of a molecular coating) that can also be controlled by suitable synthesis procedures. In this paper, by exploring the potentiality of direct micellar (DM) and high-temperature decomposition (HTD) synthesis approaches, the influence of the arrangement of nanoparticles on magnetic anisotropy and interparticle interactions has been investigated, beyond the effect of particle size. The HTD procedure allows one to obtain particles with a tendency toward cubic anisotropy ($M_r/M_s \approx 0.7$), with respect to the DM procedure, leading to particles with uniaxial anisotropy ($M_r/M_s \approx 0.4, 0.5$). The presence of an homogeneous molecular coating in $ACoFe_{HTD}$ induces the formation of self-assembly arrangement, where the interparticle distance is regulated by the thickness of the surfactant. This leads to a weaker dipolar interparticle interactions, with respect to DM samples, where the particles are in close contact. The different magnetic interaction regime induces significant changes in magnetization dynamic of nanoparticles: $ACoFe_{HTD}$ shows typical behavior of weakly interacting nanoparticles, while both DM samples exhibit a spin-glass-like behavior. The extreme versatility of the DM method permits one to obtain either randomly oriented aggregated ($IACoFe_{DM}$) or spherical iso-oriented assemblies ($SACoFe_{DM}$) $CoFe_2O_4$ nanocrystals. The formation of iso-oriented structure leads to a partial orientation of easy axis,

dx.doi.org/10.1021/cm303352r | Chem. Mater. 2013, 25, 2005−2013

inducing an increase in reduced remanent magnetization ($M_r/M_s \approx 0.4 \rightarrow M_r/M_s \approx 0.5$) and coercivity ($H_c \approx 1.17$ T $\rightarrow H_c \approx 1.45$ T) of the materials.

In conclusion, the magnetic features of magnetic nanoparticle assemblies (blocking temperatures, M_r/M_s, H_c) have been directly correlated to the synthesis conditions and nanoparticle arrangements. The fundamental nature of this study can open interesting perspectives for specific applications (hyperthermia, magnetic recording, etc.), allowing one to control the thermal stability (M_r/M_s), anisotropy (H_c), and superparamagnetic features of nanoparticle-based materials with a given particle size.

■ ASSOCIATED CONTENT

Supporting Information

This material is available free of charge via the Internet at http://pubs.acs.org.

■ AUTHOR INFORMATION

Corresponding Author

*Tel.: +39 06-90672552. Fax: +39 178 2280209. E-mail: dpeddis@hotmail.com.

Notes

The authors declare no competing financial interest.

■ REFERENCES

(1) Suber, L.; Peddis, D. Approaches to Synthesis and Characterization of Spherical and Anisometric Metal Oxide Magnetic Nanomaterials. In *Magnetic Nanomaterials*, Vol. *4*; Wiley: Weinheim, Germany, 2010.

(2) *Magnetic Properties of Fine Particles: Proceedings of the International Workshop on Studies of Magnetic Properties of Fine Particles and Their Relevance to Materials Science*, Rome, Italy, Nov. 4−8, 1991; Dormann, J. L., Fiorani, D., Eds.; North-Holland: Amsterdam, 1992.

(3) El-Hilo, M.; O'Grady, K.; Chantrell, R. W. *J. Magn. Magn. Mater.* **1992**, *114*, 307−313.

(4) Néel, L. *Ann. Geophys.* **1949**, *5*, 99−136.

(5) Peddis, D.; Cannas, C.; Musinu, A.; Piccaluga, G. *J. Phys. Chem. C* **2008**, *112*, 5141−5147.

(6) Cannas, C.; Musinu, A.; Peddis, D.; Piccaluga, G. *Chem. Mater.* **2006**, *18*, 3835−3842.

(7) Cannas, C.; Musinu, A.; Piccaluga, G.; Fiorani, D.; Peddis, D.; Rasmussen, H. K.; Mørup, S. *J. Chem. Phys.* **2006**, *125*, 164714.

(8) Pileni, M. P. *J. Phys. Chem. B* **2001**, *105*, 3358−3371.

(9) Cannas, C.; Ardu, A.; Musinu, A.; Peddis, D.; Piccaluga, G. *Chem. Mater.* **2008**, *20*, 6364−6371.

(10) Laureti, S.; Varvaro, G.; Testa, A. M.; Fiorani, D.; Agostinelli, E.; Piccaluga, G.; Musinu, A.; Peddis, D. *Nanotechnology* **2010**, *21*, 315701.

(11) Pileni, M. P. *J. Phys. D: Appl. Phys.* **2008**, *41*, 134002.

(12) Brinker, C. J. *Sol−Gel Science*; Academic Press: New York, 1990.

(13) Cannas, C.; Concas, G.; Gatteschi, D.; Falqui, A.; Musinu, A.; Piccaluga, G.; Sangregorio, C.; Spano, G. *Phys. Chem. Chem. Phys.* **2001**, *3*, 832−838.

(14) Cannas, C.; Concas, G.; Gatteschi, D.; Musinu, A.; Piccaluga, G.; Sangregorio, C. *J. Mater. Chem.* **2002**, *12*, 3141−3146.

(15) Vestal, C. R.; Zhang, Z. J. *Int. J. Nanotechnol.* **2004**, *1*, 240−263.

(16) Moumen, N.; Pileni, M. P. *Chem. Mater.* **1996**, *8*, 1128−1134.

(17) Sun, S.; Zeng, H.; Robinson, D. B.; Raoux, S.; Rice, P. M.; Wang, S. X.; Li, G. *J. Am. Chem. Soc.* **2004**, *126*, 273−279.

(18) Cannas, C.; Gatteschi, D.; Musinu, A.; Piccaluga, G.; Sangregorio, C. *J. Phys. Chem. B* **1998**, *102*, 7721−7726.

(19) Hyeon, T. *Chem. Commun.* **2003**, 927−934.

(20) Feltin, N.; Pileni, M. P. *Langmuir* **1997**, *13*, 3927−3933.

(21) Cannas, C.; Ardu, A.; Peddis, D.; Sangregorio, C.; Piccaluga, G.; Musinu, A. *J. Colloid Interface Sci.* **2010**, *342*, 415−422.

(22) Cannas, C.; Musinu, A.; Ardu, A.; Orrù, F.; Peddis, D.; Casu, M.; Sanna, R.; Angius, F.; Diaz, G.; Piccaluga, G. *Chem. Mater.* **2010**, *22*, 3353−3361.

(23) Sun, S.; Zeng, H. *J. Am. Chem. Soc.* **2002**, *124*, 8204−8205.

(24) Peddis, D.; Orrù, F.; Ardu, A.; Cannas, C.; Musinu, A.; Piccaluga, G. *Chem. Mater.* **2012**, *24*, 1062−1071.

(25) West, A. R. *Solid State Chemistry and Its Applications*; John Wiley and Sons: Chichester, U.K., 1984.

(26) Hansen, M. F.; Mørup, S. *J. Magn. Magn. Mater.* **1999**, *203*, 214−216.

(27) Del Bianco, L.; Fiorani, D.; Testa, A. M.; Bonetti, E.; Savini, L.; Signoretti, S. *Phys. Rev. B* **2002**, *66*, 174418−174429.

(28) Hansen, M. F.; Mørup, S. *J. Magn. Magn. Mater.* **1998**, *184*, 262−274.

(29) Dormann, J. L.; Fiorani, D.; Tronc, E. Magnetic relaxation in fine particle systems. In *Advances in Chemical Physics*, Vol. XCVIII; New York; 1997.

(30) Geshev, J.; Mikhov, M.; Schmidt, J. E. *J. Appl. Phys.* **1999**, *85*, 7321−7327.

(31) Peddis, D.; Cannas, C.; Musinu, A.; Piccaluga, G. *Chem.—Eur. J.* **2009**, *15*, 7822−7829.

(32) Garcia-Otero, J.; Porto, M.; Rivas, J.; Bunde, A. *J. Appl. Phys.* **1999**, *85*, 2287−2292.

(33) Batlle, X.; García del Muro, M.; Labarta, A. *Phys. Rev. B* **1997**, *55*, 6440.

(34) Morup, S.; Hansen, M. F.; Frandsen, C. *Beilstein J. Nanotechnol.* **2010**, *1*, 182−190.

(35) Bedanta, S.; Kleeman, W. *J. Phys. D: Appl. Phys.* **2009**, *42*, 013001.

(36) Tholence, J. L. *Magnetic Susceptibility of Superconductors and Other Spin Systems*; Plenum Press: New York, 1991.

(37) Saslow, W. M. *Phys. Rev. B* **1988**, *37*, 676.

(38) Winkler, E.; Zysler, R. D.; Vasquez Mansilla, M.; Fiorani, D.; Rinaldi, D.; Vasilakaki, M.; Trohidou, K. N. *Nanotechnology* **2008**, *19*, 185702.

(39) Parker, D.; Dupuis, V.; Ladieu, F.; Bouchaud, J. P.; Dubois, E.; Perzynski, R.; Vincent, E. *Phys. Rev. B* **2008**, *77*, 104428−104429.

(40) Dormann, J. L.; Fiorani, D.; Tronc, E. *J. Magn. Magn. Mater.* **1999**, *202*, 251−267.

(41) Slonczewski, J. C. *J. Appl. Phys.* **1961**, *32*, S253−S263.

(42) Virden, A.; Wells, S.; O'Grady, K. *J. Magn. Magn. Mater.* **2007**, *316*, e768−e771.

(43) Usov, N. A.; Peschany, S. E. *J. Magn. Magn. Mater.* **1997**, *174*, 247−260.

(44) Geshev, J.; Mikhov, M. *J. Magn. Magn. Mater.* **1992**, *104−107*, 1569−1570.

(45) Kodama, R. H.; Berkowitz, A. E.; McNiff, J. E. J.; Foner, S. *Phys. Rev. Lett.* **1996**, *77*, 394−397.

(46) Morrish, A. H. *The Physical Principles of Magnetism*; Wiley: New York, 1965.